Analytical model for arbitrarily configured neighboring shallow geothermal installations in the presence of groundwater flow

Al-Khoury, Rafid; BniLam, Noori; Arzanfudi, Mehdi M.; Saeid, Sanaz

DOI
10.1016/j.geothermics.2021.102063

Publication date
2021

Document Version
Final published version

Published in
Geothermics

Citation (APA)
Al-Khoury, R., BniLam, N., Arzanfudi, M. M., & Saeid, S. (2021). Analytical model for arbitrarily configured neighboring shallow geothermal installations in the presence of groundwater flow. *Geothermics*, *93*, 1-11. Article 102063. https://doi.org/10.1016/j.geothermics.2021.102063

Geothermics 93 (2021) 102063

Contents lists available at ScienceDirect

Geothermics

journal homepage: www.elsevier.com/locate/geothermics

Analytical model for arbitrarily configured neighboring shallow geothermal installations in the presence of groundwater flow

Rafid Al-Khoury [a,*], Noori BniLam [b], Mehdi M. Arzanfudi [a,c], Sanaz Saeid [a]

[a] Faculty of Civil Engineering and Geosciences, Computational Mechanics Chair, Delft University of Technology, P.O. Box 5048, 2600 GA, Delft, the Netherlands
[b] University of Antwerp – imec, IDLab - Faculty of Applied Engineering, Sint-Pietersvliet 7, 2000, Antwerp, Belgium
[c] DIANA FEA BV., Thijsseweg 11, 2629JA, Delft, the Netherlands

ARTICLE INFO

Keywords:
Moving cylindrical heat source
Conduction-convection heat flow
Heat flow due to groundwater
Neighboring ground source heat pump installations

ABSTRACT

This paper introduces an analytical model analyzing the effect of groundwater flow on heat transfer in an infinite conductive-convective porous domain representing shallow geothermal systems with arbitrarily configured cylindrical heat sources. The model is formulated based on the moving source concept and solved based on the spectral analysis method and the superposition principle. Compared to models based on the Green's function and the Laplace transform, the proposed spectral model has a simpler formulation, computationally efficient and easy to implement in computer codes. It can handle random time-dependent thermal loads and any arbitrarily configured grid distribution. The verification and numerical examples demonstrate the computational capabilities of the model, and show how the groundwater flow can play an important role in the thermal interaction between heat sources. They also feature how to make use of the direction of groundwater flow to avoid undesirable thermal interaction between neighboring installations, rapid depletion of energy sources and unfair mining of geothermal energy.

1. Introduction

Groundwater flow in subsurface formations can have a notable effect on the amount of energy gained from shallow geothermal systems, and on the extent of thermal interactions between heat sources. The significance of the heat gain due to groundwater flow and the thermal interactions between heat sources is highly manifested in the ground source heat pump (GSHP) technology, which normally involves neighboring heat sources and installations consisting of arbitrarily configured borehole heat exchangers (BHE). It primarily comprises vertical boreholes that might go as deep as 300 m in the ground where the presence of groundwater is very likely. This technology is appealing because it makes use of free, moderate temperatures at shallow depths to produce efficient and clean energy suitable for heating and cooling of buildings.

As the demand for green energy is increasing, the use of GSHP technology has been multiplied in recent years. However, despite its advantages in mitigating the CO_2 emissions, utilization of this technology in densely populated areas incorporating neighbouring installations can cause undesirable thermal interaction between boreholes, rapid depletion of energy sources and unfair mining of geothermal energy. In the presence of groundwater flow these problems become more challenging and require careful treatment. As such, the configuration of GSHP systems and their distances from nearby installations have become essential measures in designing regional shallow geothermal systems.

Modeling conduction-convection in a multiple heat sources GSHP system involves two main computational aspects: 1) modeling heat convection due to groundwater flow in a low enthalpy porous domain, and 2) modeling thermal interactions in regions consisting of neighboring grids with different configurations and thermal loads. In general, the numerical methods are equipped to tackle these two aspects in a rather straightforward procedure. Solving the heat equation in a low enthalpy porous domain can readily be made by a relatively simple discretization procedure, and the coupling between multiple heat sources is automatically done via a proper gridding/meshing of the geometry. The finite element method and the finite difference/volume method have been widely utilized for simulating GSHP systems constituting multiple borehole heat exchangers embedded in soil layers with groundwater flow. COMSOL Multiphysics (COMSOL, 2019), FEFLOW finite element package (FEFLOW, 2020) and TOUGH2 finite difference code (Pruess et al., 1999) are the most commonly utilized commercial tools for this purpose. Many other academic tools have been introduced

* Corresponding author.
E-mail address: r.i.n.alkhoury@tudelft.nl (R. Al-Khoury).

https://doi.org/10.1016/j.geothermics.2021.102063
Received 25 October 2020; Received in revised form 6 January 2021; Accepted 8 February 2021
Available online 23 February 2021

for analysing conductive-convective heat flow in GSHP systems. Among others, Al-Khoury et al. (2005) and Nam et al. (2008) utilized the finite element method for this purpose; Yavuzturk et al. (1999) and Nabi and Al-Khoury (2012a,b) utilized the finite volume method; and Cimmino and Baliga (2019) utilized the control-volume finite element method (CVFEM), which is a hybrid between the finite element method and the finite volume method. These tools can provide advanced numerical features, but are computationally demanding, making the analytical methods more appealing for engineering practice.

The analytical methods, however, are more intricate in solving the governing heat equations. They are not by-definition equipped to tackle these two aspects, and the solution has to be tailored to the physics of the problem (1D, 2D or 3D), the geometry of the heat source (line or cylindrical), the kind of boundary conditions (Dirichlet or Neumann) and whether the domain encompasses a single or multiple heat sources. Each of these modeling features needs a special treatment. Carslaw and Jaeger (1959) were among the firsts to introduce analytical solutions to heat conduction-convection problems using the moving heat source concept. They provided analytical solutions to the moving infinite line heat source using the Green's function method, and to the moving infinite cylindrical heat source using the Laplace transform. Diao et al. (2004) and Capozza et al. (2013) adopted Carslaw and Jaeger's Green's function solution for the moving infinite line source to simulate heat flow in GSHP systems in the presence of groundwater flow and multiple heat sources. Erol et al. (2015) extended the moving infinite line source to a moving finite line source in a pseudo 3D domain encompassing multiple heat sources using the Green's function method. In these works, the superposition principle for the Neumann boundary condition has been adopted to couple the effect of the heat sources. To our knowledge, no analytical models have yet been introduced for moving multiple cylindrical heat sources specifically applied to the GSHP systems. The essence of considering a cylindrical heat source rather than a line is that it is a better representation of the borehole heat exchanger, which is on average 12 cm in diameter. With the presence of groundwater flow, appropriate representation of the heat source geometry becomes even more essential.

Here we present an analytical model capable of analyzing lateral heat conduction-convection in areas consisting of arbitrarily distributed cylindrical heat sources with random time-dependent thermal loads. The heat flow is analyzed in a 2D, $xy-$ plane, shown schematically in Fig. 1a. The model is formulated based on the moving source concept and solved based on the spectral analysis method and the superposition principle. The spectral analysis is utilized to solve the heat equation for a single cylindrical heat source subjected to Dirichlet (prescribed temperature) and Neumann (prescribed heat flux) boundary conditions in the presence of groundwater flow (Fig. 1b). And the superposition principle is utilized to couple the heat equations for multiple heat sources. The spectral analysis is a powerful method for solving linear initial and boundary value problems. It makes use of the eigenfunction expansion for decomposing relatively complicated functions into simpler basic functions such as the trigonometric or exponential functions. It also makes use of the fast Fourier transform (FFT) for transforming partial differential equations expressed in the time domain to ordinary differential equations expressed in the frequency domain (Doyle, 1997; Al-Khoury, 2012). This combination brings about solutions given in series summations which are ideal for computer implementation; and allows analysing any arbitrarily measured input data in an exceptionally efficient manner. The novelty of the resulting spectral model, compared to existing analytical models, can be summarized as follows:

1 It can handle multiple cylindrical heat sources rather than line heat sources.
2 It can simulate any arbitrarily configured heat sources with no special treatment for corner or middle heat sources.
3 It is stable and computationally efficient in dealing with any number of heat sources and any time-dependent thermal load scenarios. It is also stable in analyzing heat flow for a wide range of groundwater flow velocities.

2. Single cylindrical heat source: Spectral analysis

The governing equation of heat conduction-convection in an infinite, homogeneous, isotropic domain, moving with velocity $-U$ along the x -axis, can be expressed as

$$\frac{\partial^2 T}{\partial x^2}+\frac{\partial^2 T}{\partial y^2}+\frac{U}{\alpha}\frac{\partial T}{\partial x}-\frac{1}{\alpha}\frac{\partial T}{\partial t}=0 \tag{1}$$

in which $T\equiv T(x,y,t)$ is the temperature (K) in an $xy-$ plane, and $\alpha=\lambda/(\rho c)$ is the material thermal diffusivity (m^2/s) with λ the thermal conductivity (W/(m.K)), ρ the mass density (kg/m^3) and c the specific heat capacity (J/(kg.K)).

The domain encompasses a single cylindrical heat source with radius a. It is initially at zero temperature, and for times $t>0$ the domain is subjected to Dirichlet or Neumann boundary conditions at $x^2+y^2=a^2$ (see Fig. 1b). The Dirichlet boundary condition entails

$$T(a,\theta,t)=T_{\text{in}}(t) \tag{2}$$

where $T_{\text{in}}(t)$ is any time-dependent temperature signal; and the Neumann boundary condition implies

$$-2\pi a\lambda\left.\frac{\partial T(r,\theta,t)}{\partial r}\right|_{r=a}=Q_{\text{in}}(t) \tag{3}$$

where $Q_{\text{in}}(t)$ is any time-dependent heat flux signal, and r,θ are the polar coordinates of the cylindrical heat source.

Since the cylindrical cross section is periodic (continuous) in the azimuth ($\theta-$ direction), the following physical constraints are maintained:

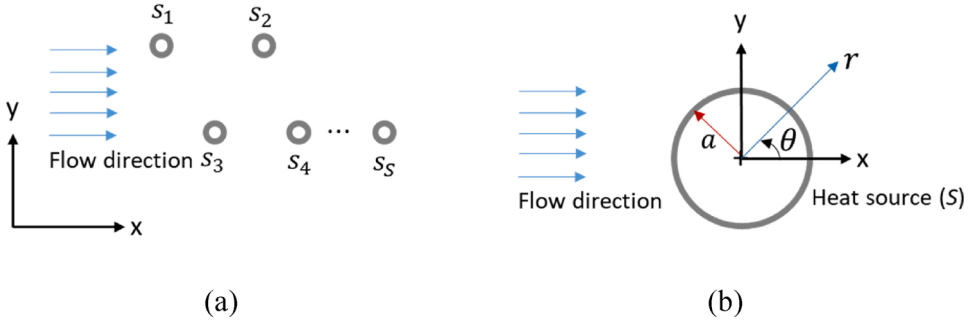

Fig. 1. a) A schematic representation of the physical domain; b) Single heat source.

$$T(a,\theta,t) = T(a,\theta+2\pi,t) \tag{4}$$

$$-2\pi a\lambda \frac{\partial T(r,\theta,t)}{\partial r}\bigg|_{r=a} = -2\pi a\lambda \frac{\partial T(r,\theta+2\pi,t)}{\partial r}\bigg|_{r=a}$$

The solution of the above initial and boundary value problem is undertaken using the Fourier series for the spatial domain and the fast Fourier transform (FFT) for the temporal domain. Details of the solution is given in Al-Khoury et al. (2020). Here, we give a brief description of the derivation and solution, to be utilized for formulating the superposition equations given in Section 3.

Eq. (1) is best expressed in the polar coordinate system in $xy-$ plane, giving

$$\frac{\partial^2 u}{\partial r^2} + \frac{1}{r}\frac{\partial u}{\partial r} + \frac{1}{r^2}\frac{\partial^2 u}{\partial \theta^2} - \frac{U^2}{4\alpha^2}u - \frac{1}{\alpha}\frac{\partial u}{\partial t} = 0 \tag{5}$$

with

$$u \equiv u(r,\theta,t) = T(t)e^{Ur\cos\theta/2\alpha} \tag{6}$$

The spectral analysis is utilized to solve this equation, giving

$$T(r,\theta,t) = \sum_m \sum_n \widehat{u}_n(r,\theta,\omega_m)\, e^{-Ur\cos\theta/2\alpha} e^{i\omega_m t} \tag{7}$$

where, for the Dirichlet boundary condition:

$$\widehat{u}(r,\theta,\omega) = \sum_n \varepsilon_n \frac{\widehat{T}_{\text{in}}(\omega)}{K_n(qa)} I_n\left(\frac{Ua}{2\alpha}\right)\cos n\theta K_n(qr)\ ;\ n=0,1,2,\cdots \varepsilon_0 = 1;\ \varepsilon_n = 2 \text{ for } n \geq 1 \tag{8}$$

with

$$q = \left(\frac{U^2}{4\alpha^2} + \frac{i\omega}{\alpha}\right)^{1/2} \tag{9}$$

and for the Neumann boundary condition, the solution is:

$$\widehat{u}(r,\theta,\omega) = \sum_n a_n \cos n\theta\, K_n(qr) \quad ; \quad n = 0,\ 1,\ 2,\cdots \tag{10}$$

with

$$\begin{aligned} a_0 &= \frac{1}{2\pi}\int_0^{2\pi} f(\theta)\, d\theta \quad ; \quad n = 0 \\ a_n &= \frac{1}{\pi}\int_0^{2\pi} f(\theta)\cos n\theta\, d\theta \quad ; \quad n \geq 1 \end{aligned} \tag{11}$$

in which

$$f(\theta) = \frac{\alpha\, \widehat{Q}_{\text{in}}(\omega) e^{Ua\cos\theta/2\alpha}}{\pi\lambda(K_n(qa)Ua\cos\theta + 2K_{n+1}(qa)\alpha qa - 2K_n(qa)\alpha\, n)} \tag{12}$$

In the above equations, ω is the angular frequency, subscript m is the FFT frequency counter, and I_n and K_n are the modified Bessel functions of the first and second kinds of order n, respectively. The inner summation over n in Eq. (7) is the Fourier series solution of the spatial domain, and the outer summation over m is the inverse FFT for reconstructing the time domain from the frequency domain.

3. Multiple cylindrical heat sources: Superposition formulation

Eqs. (7)–(12) describe the temperature distribution in an infinite conductive-convective solid domain subjected to a cylindrical heat source with Dirichlet and Neumann boundary conditions. As the system is linear, the superposition principle can be utilized to simulate heat flow in a multiple heat sources domain. Almost all current finite and infinite line heat sources used in shallow geothermal engineering, such as those referred to in Section 1, utilize the superposition principle for the Neumann boundary condition. Little work has been allocated for the Dirichlet boundary condition. A notable one is the model introduced by Pasquier and Marcotte (2013) who adopted an iterative algorithm to describe heat flow in a multiple heat sources domain, though only conduction heat flow was considered.

3.1. Multiple heat sources with Neumann boundary condition

The superposition principle for the Neumann boundary condition implies algebraic summation over temperatures exerted by the individual heat sources on a point in space and time (referred to as the reference point in Fig. 2), such that

$$T(r,\theta,t) = \sum_s \sum_m \sum_n \widehat{u}_{n|s}(r_s,\theta_s,\omega_m)\, e^{-U\, r_s\cos\theta_s/2\alpha} e^{i\omega_m t} \tag{13}$$

where the subscript s denotes the heat source number, r_s is the distance from heat source s to the reference point, θ_s is the angle between the source and the reference point (see Fig. 2), and $\widehat{u}_{n|s}(r_s,\theta_s,\omega_m)$ is as given in Eqs. (10)–(12).

3.2. Multiple heat sources with Dirichlet boundary condition

The algebraic sum in the Neumann case is not directly applicable to the Dirichlet boundary condition, as the explicit summation of temperatures exerted by the heat sources would give an unphysical increase or decrease of temperature at the reference point (BniLam and Al-Khoury, 2016). Here, the heat sources must be coupled such that the prescribed temperature at the heat source is adjusted by the temperatures exerted by the neighboring heat sources.

For a single heat source (s), the temperature at a reference point in the domain making a radial distance r_s and an angle θ_s from the heat source (Fig. 2) is given by Eq. (7), which is, in the frequency domain, expressed as

$$\widehat{T}(r_s,\theta_s,\omega) = \sum_n \widehat{u}_n(r_s,\theta_s,\omega) e^{-Ur_s\cos\theta_s/2\alpha} \tag{14}$$

The spectral analysis for the Dirichlet boundary condition for a single heat source is given in Eq. (8), which upon substituting in Eq. (14) gives

$$\widehat{T}(r_s,\theta_s,\omega) = A_s R_s e^{-Ur_s\cos\theta_s/2\alpha} \tag{15}$$

in which

$$R_s = \sum_n \varepsilon_n \frac{1}{K_n(qa_s)} I_n\left(\frac{Ua_s}{2\alpha}\right)\cos n\theta_s\ K_n(qr_s) \tag{16}$$

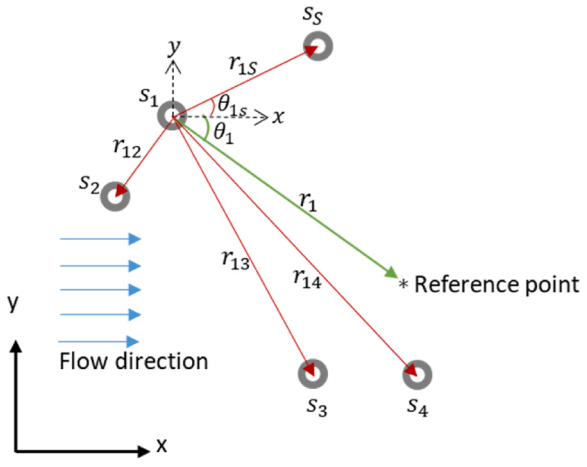

Fig. 2. Symbols and terms.

and A_s is the temperature amplitude at the heat source, equals, in a single heat source domain, to $\widehat{T}_{\text{in}}$ (see Eq. (8)). However, in a multiple heat sources domain, the amplitude at a heat source in the domain needs to be adjusted by the temperatures exerted by neighboring heat sources, such that, for heat source s, it reads:

$$\widehat{T}(a_s,\theta_s,\omega)=A_s \tag{17}$$

Following this, the temperature at a reference point in a multiple heat sources domain is expressed as

$$\widehat{T}(r,\theta,\omega)=A_1R_1e^{-Ur_1\cos\theta_1/2\alpha}+A_2R_2e^{-Ur_2\cos\theta_2/2\alpha}+\cdots+A_SR_Se^{-Ur_S\cos\theta_S/2\alpha} \tag{18}$$

where $r_1,\ r_2,\ \ldots r_S$ are the radial distances between the reference point and the heat sources $s_1,\ s_2,\ldots s_S$ respectively (Fig. 2), and $A_1,\ A_2,\ \ldots A_S$ are their associated adjusted amplitudes.

Solving Eq. (18) at the heat source boundary for all heat sources (discarding the dependent variables (r,θ,ω) for easy notation), considering Eq. (17), yields

$$\begin{aligned}
\widehat{T}_{\text{in1}} &= A_1 && && A_2R_{12}e^{-Ur_{12}\cos\theta_{12}/2\alpha} && +\cdots+A_SR_{1S}e^{-Ur_{1S}\cos\theta_{1S}/2\alpha}\\
\widehat{T}_{\text{in2}} &= A_1R_{21}e^{-Ur_{21}\cos\theta_{21}/2\alpha} && +A_2 && && \cdots+A_SR_{2S}e^{-Ur_{2S}\cos\theta_{2S}/2\alpha}\\
&\ \ \vdots\\
\widehat{T}_{\text{inS}} &= A_1R_{S1}e^{-Ur_{S1}\cos\theta_{S1}/2\alpha} && +A_2R_{S2}e^{-Ur_{S2}\cos\theta_{S2}/2\alpha} && +\cdots+A_S
\end{aligned} \tag{19}$$

in which $\widehat{T}_{\text{in1}}$ is the prescribed temperature at heat source 1, etc., r_{12} is the radial distance between heat source 1 and heat source 2, etc. and θ_{12} is the angle between heat source 1 and heat source 2, etc. (Fig. 2). This set of equations indicates that the prescribed temperature at heat source 1 (for instance) $\widehat{T}_{\text{in1}}$ is equal to its adjusted temperature amplitude at its boundary A_1 plus temperatures exerted by all neighbouring heat sources, which themselves experienced adjustment of their temperature amplitudes.

In a matrix format, Eq. (19) is expressed as

$$\begin{pmatrix}\widehat{T}_{\text{in1}}\\ \widehat{T}_{\text{in2}}\\ \vdots\\ \widehat{T}_{\text{inS}}\end{pmatrix}=\begin{pmatrix}1 & R_{12}e^{-Ur_{12}\cos\theta_{12}/2\alpha} & \cdots & R_{1S}e^{-Ur_{1S}\cos\theta_{1S}/2\alpha}\\ R_{21}e^{-Ur_{21}\cos\theta_{21}/2\alpha} & 1 & \cdots & R_{2S}e^{-Ur_{2S}\cos\theta_{2S}/2\alpha}\\ \vdots & \vdots & \vdots & \vdots\\ R_{S1}e^{-Ur_{S1}\cos\theta_{S1}/2\alpha} & R_{S2}e^{-Ur_{S2}\cos\theta_{S2}/2\alpha} & \cdots & 1\end{pmatrix}\begin{pmatrix}A_1\\ A_2\\ \vdots\\ A_S\end{pmatrix} \tag{20}$$

Solving Eq. (20) for vector $\boldsymbol{A}$, yields

$$\begin{pmatrix}A_1\\ A_2\\ \vdots\\ A_S\end{pmatrix}=\begin{pmatrix}1 & R_{12}e^{-Ur_{12}\cos\theta_{12}/2\alpha} & \cdots & R_{1S}e^{-Ur_{1S}\cos\theta_{1S}/2\alpha}\\ R_{21}e^{-Ur_{21}\cos\theta_{21}/2\alpha} & 1 & \cdots & R_{2S}e^{-Ur_{2S}\cos\theta_{2S}/2\alpha}\\ \vdots & \vdots & \vdots & \vdots\\ R_{S1}e^{-Ur_{S1}\cos\theta_{S1}/2\alpha} & R_{S2}e^{-Ur_{S2}\cos\theta_{S2}/2\alpha} & \cdots & 1\end{pmatrix}^{-1}\begin{pmatrix}\widehat{T}_{\text{in1}}\\ \widehat{T}_{\text{in2}}\\ \vdots\\ \widehat{T}_{\text{inS}}\end{pmatrix} \tag{21}$$

Solving Eq. (21) and substituting the resulting amplitudes into Eq. (18), the general solution in the time domain can then be obtained using the inverse fast Fourier transform (IFFT), as

$$T(r,\theta,t)=\sum_m\sum_s A_sR_s(r_s,\theta_s,\omega_m)e^{-Ur_s\cos\theta_s/2\alpha}e^{i\omega_mt} \tag{22}$$

This equation gives the temperature at a reference point in the domain that is at a distance r_s from each of the heat sources and making an angle θ_s with them (Fig. 2). To make contour plots, such as those given in Figs. 5 and 9, Eq. (22) is solved for $0\le\theta_s\le 359$ in a relatively dense $xy-$ grid of reference points.

As it can be observed from the above formulation, using the matrix technique allows coupling heat sources with any arbitrary configurations and thermal loads. There is no special treatment for corner or middle heat sources, the boreholes can have any diameter and flow rates, and the use of the FFT algorithm allows applying any thermal load scenarios.

4. Model verification

We use the finite element method to verify the accuracy of the proposed spectral model. For this purpose a two-dimensional, fully saturated porous domain constituting a solid phase and a water phase is considered. The domain includes nine cylindrical heat sources, 5 m apart from each other (Fig. 3). The geometry resembles a soil layer with a lateral groundwater flow passing through borehole heat exchangers. The domain is in local thermal equilibrium and the heat equation is averaged over the constituents, such that

$$\frac{\partial^2T}{\partial x^2}+\frac{\partial^2T}{\partial y^2}+\frac{U_{\text{eff}}}{\alpha_{\text{eff}}}\frac{\partial T}{\partial x}-\frac{1}{\alpha_{\text{eff}}}\frac{\partial T}{\partial t}=0 \tag{23}$$

where

$$\begin{aligned}
\alpha_{\text{eff}} &= \frac{\lambda_{\text{eff}}}{\rho c_{\text{eff}}}\\
\lambda_{\text{eff}} &= \varphi\lambda_w+(1-\varphi)\lambda_s\\
\rho c_{\text{eff}} &= \varphi\rho_wc_w+(1-\varphi)\rho_sc_s
\end{aligned} \tag{24}$$

and

$$U_{\text{eff}}=\frac{\varphi\rho_wc_w}{\rho c_{\text{eff}}}U \tag{25}$$

in which the subscripts $w,\ s,$ eff denote the water phase, the solid matrix and the effective parameter, respectively; φ is the porosity and U_{eff} is termed the thermal retardation factor. The thermo-physical parameters of the porous domain are given in Table 1.

The initial and boundary conditions are:

$$\begin{aligned}
T_{\text{initial}} &= 0\ ^\circ C && ; && t=0\\
T_{\text{in}} &= \begin{cases}0\ ^\circ C-10\ ^\circ C\\ 10\ ^\circ C\end{cases} && ; && \begin{matrix}0\le t\le 10\ d\\ 0\le t\le 10\ d\end{matrix}\ ;\ \text{Dirichlet case}\\
Q_{\text{in}} &= \begin{cases}0\ \text{W/m}-100\ \text{W/m}\\ 100\ \text{W/m}\end{cases} && ; && \begin{matrix}0\le t\le 10\ d\\ t>10\ d\end{matrix}\ ;\ \text{Neumann case}
\end{aligned} \tag{26}$$

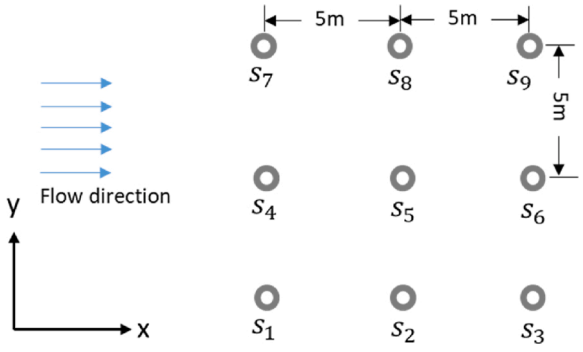

Fig. 3. Heat sources configuration.

Table 1
Physical and thermal parameters.

parameter	magnitude	unit
Solid mass density (ρ_s)	2650	kg/m^3
Solid specific heat (c_s)	900	J/kg.K
Solid thermal conductivity (λ_s)	2.5	W/m.K
Water mass density (ρ_w)	1000	kg/m^3
Water specific heat (c_w)	4180	J/kg.K
Water thermal conductivity (λ_w)	0.56	W/m.K
Porosity (φ)	0.2	–
Water flow velocity	1e-5	m/s
Heat source radius (a)	0.1	m

Computational results obtained from the spectral model are compared to those obtained from the finite element package: Multi-physics, Multidomain, Multiphase finite element analysis, MMM-FEM, developed at Delft University of Technology (Arzanfudi et al., 2020).

The finite element domain is 90 m × 60 m, encompassing 9 cylindrical heat sources with radius 0.1 m; but due to symmetry, only half of the domain is modeled. The finite element mesh consists of 9391, 2D 4-node quadrilateral elements with a minimum size of 0.0104 m along the heat sources circumferences. The top view of the mesh with a zoom around the heat sources is shown in Fig. 4.

Fig. 5 shows the temperature contours for both models after 50 and 100 days of operation for the Dirichlet boundary condition case. The figure clearly shows a very good matching between the spectral model and the finite element model.

Fig. 6 shows the temperature contours of the same analysis but for the Neumann boundary condition. As for the Dirichlet case, the figure shows a very good matching between the two models.

5. Thermal interactions in arbitrarily configured cylindrical heat sources: a numerical example

This numerical example is meant to demonstrate the computational capabilities of the proposed spectral model in simulating conduction-convection heat flow in a porous domain subjected to arbitrarily configured cylindrical heat sources. It is also meant to highlight the physics of such a system and show how the groundwater flow can increase or decrease the thermal interaction between the heat sources.

The heat sources are assumed to be distributed into two GSHP installations with different configurations, as shown in Fig. 7. GSHP 1 consists of 5 cylindrical heat sources and GSHP 2 consists of 4 cylindrical heat sources. This configuration highlights the capability of the model to simulate unsymmetrical distribution of heat sources with no special treatment for corner or middle heat source. The material and physical parameters are given in Table 1. We apply the Neumann boundary condition on the heat sources, as it is physically more realistic to describe operating GSHP systems. The two GSHP systems operate for 12 months with thermal loads varying between +50 W/m and -50 W/m, as shown in Fig. 8. During the day, the two systems are ON between 08:00

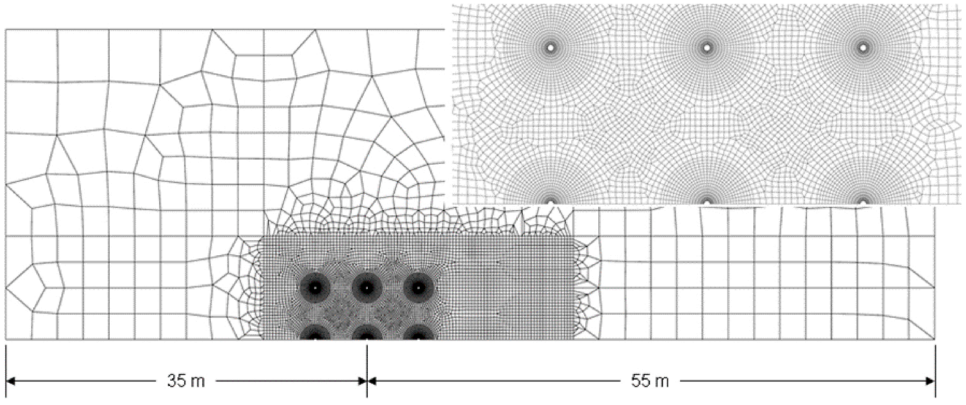

Fig. 4. Top view of the finite element mesh with a zoom around the heat sources.

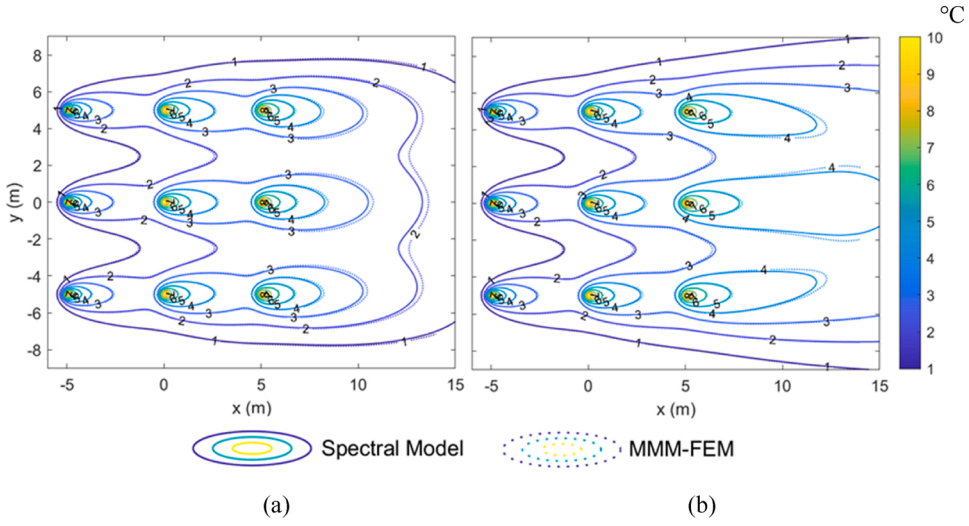

Fig. 5. Spectral model versus finite element model for the Dirichlet boundary condition case: a) 50 days; b) 100 days.

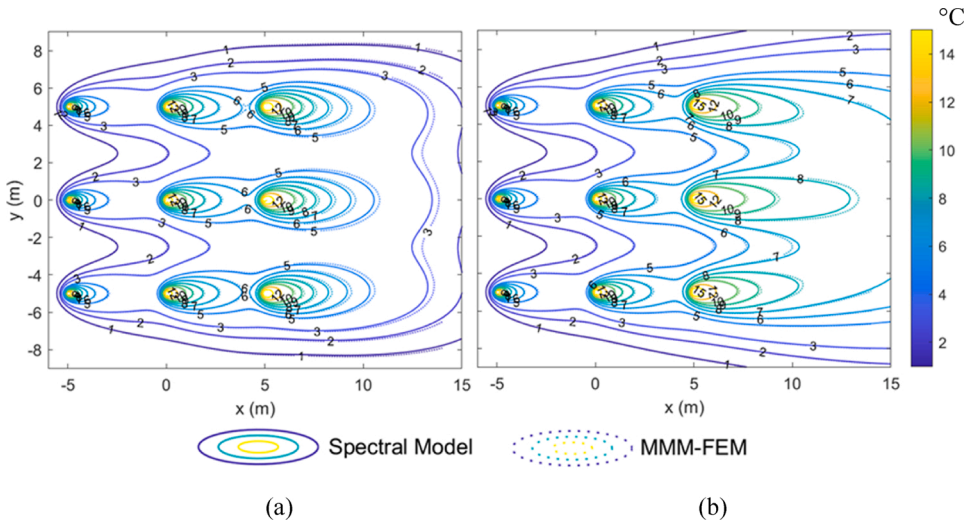

Fig. 6. Spectral model versus finite element model for the Neumann boundary condition case: a) 50 days; b) 100 days.

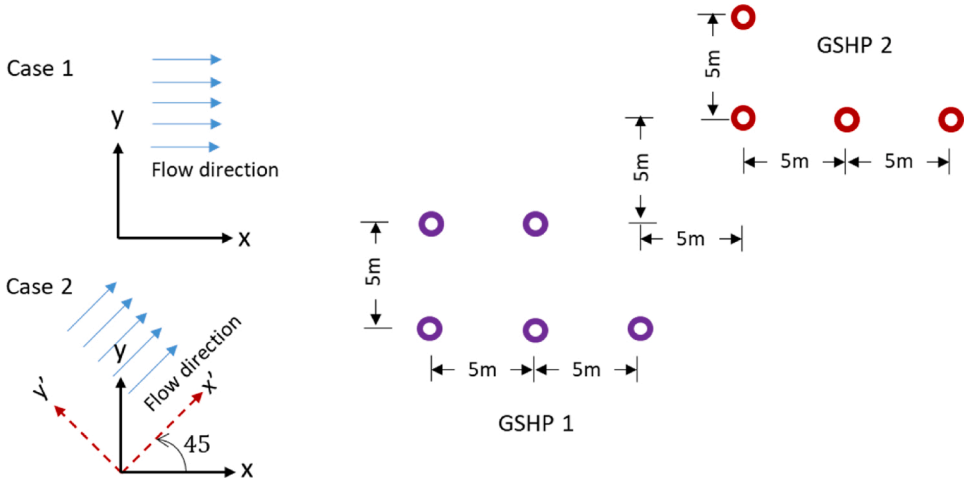

Fig. 7. Two GSHP installations with different configurations. Case 1: flow direction 0° with x-axis; Case 2: flow direction 45° with x-axis.

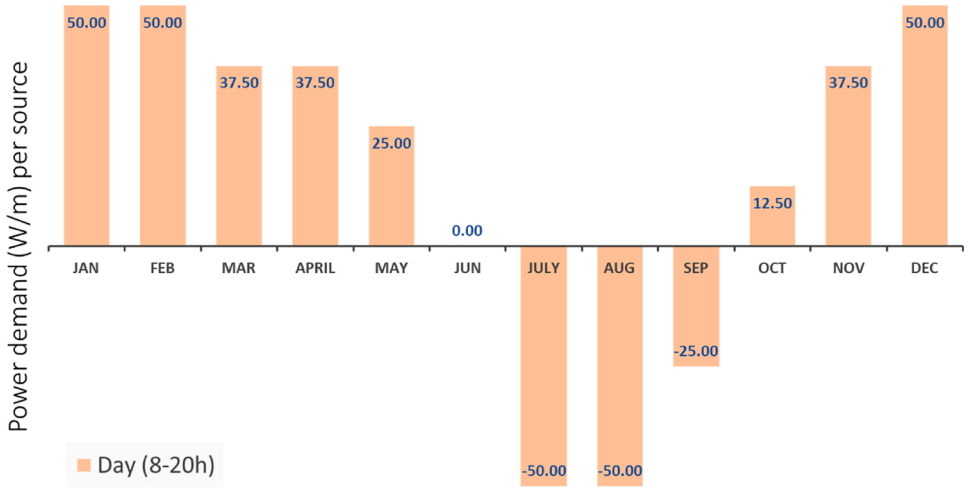

Fig. 8. Operating thermal loads scenario for the individual heat sources.

and 20:00 hours, and OFF for the rest of the day.

The following three cases have been examined:

1. Case 1: groundwater flow along the x-axis.
2. Case 2: groundwater flow making an angle 45° from the x-axis.
3. Case 3: GSHP 1 extracting ± 75 W/m instead of ± 50 W/m.

Case 1:groundwater flow along the *x*-axis

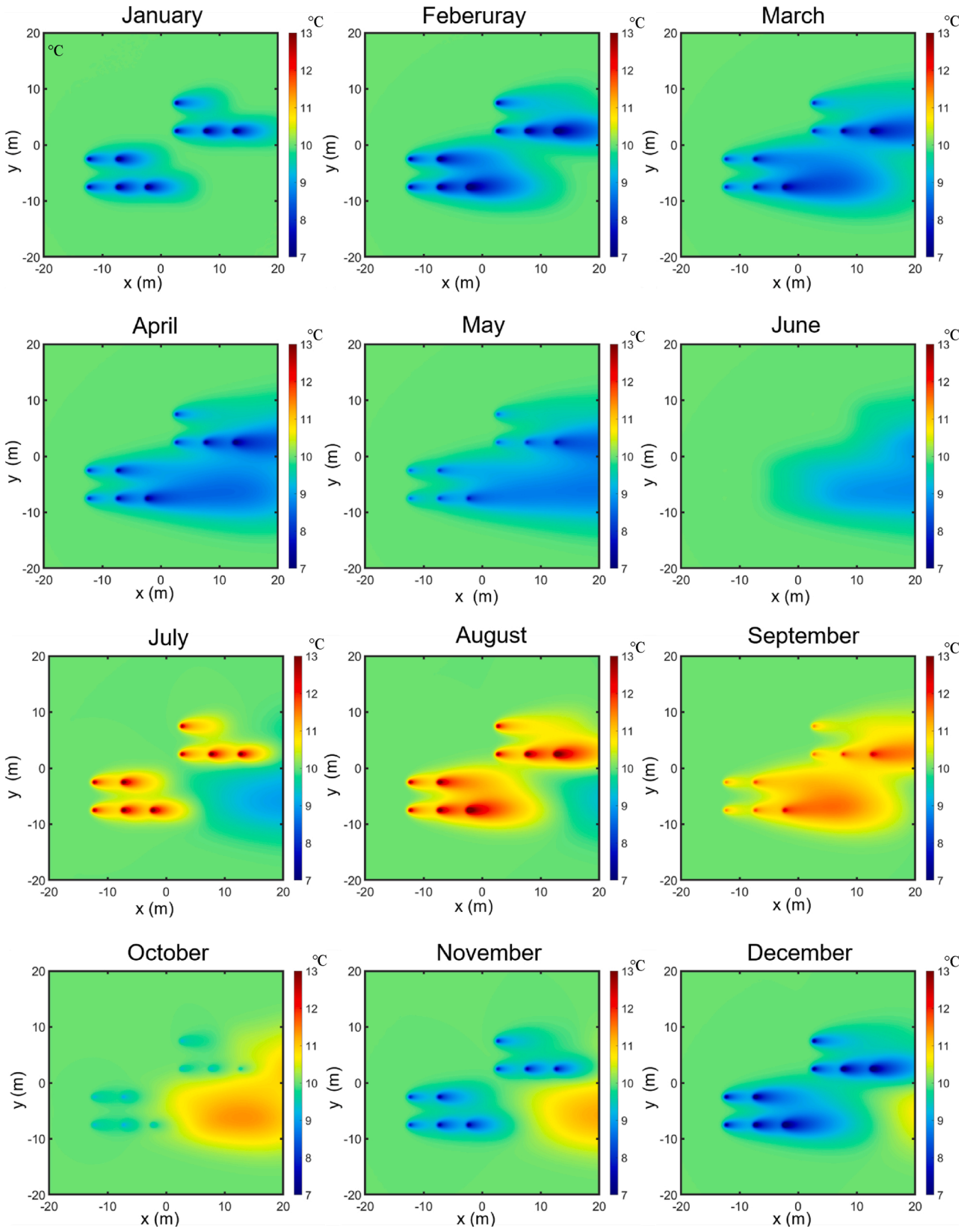

Fig. 9. Monthly temperature distribution for Case 1: groundwater flow along the *x*-axis.

Fig. 9 shows the computed temperature distribution for Case 1, for 12 months. The figure signifies the fluctuation of the temperature in the soil mass with the operation scenario of the months (Fig. 8), and shows the affected areas due to the combined effect of the heat sources. Remarkably, it displays plumes of heat moving in times when the operation stops or changes modes, as can be seen in June, July and August for the cold plume (in blue); and in October, November and December for the hot plume (in red).

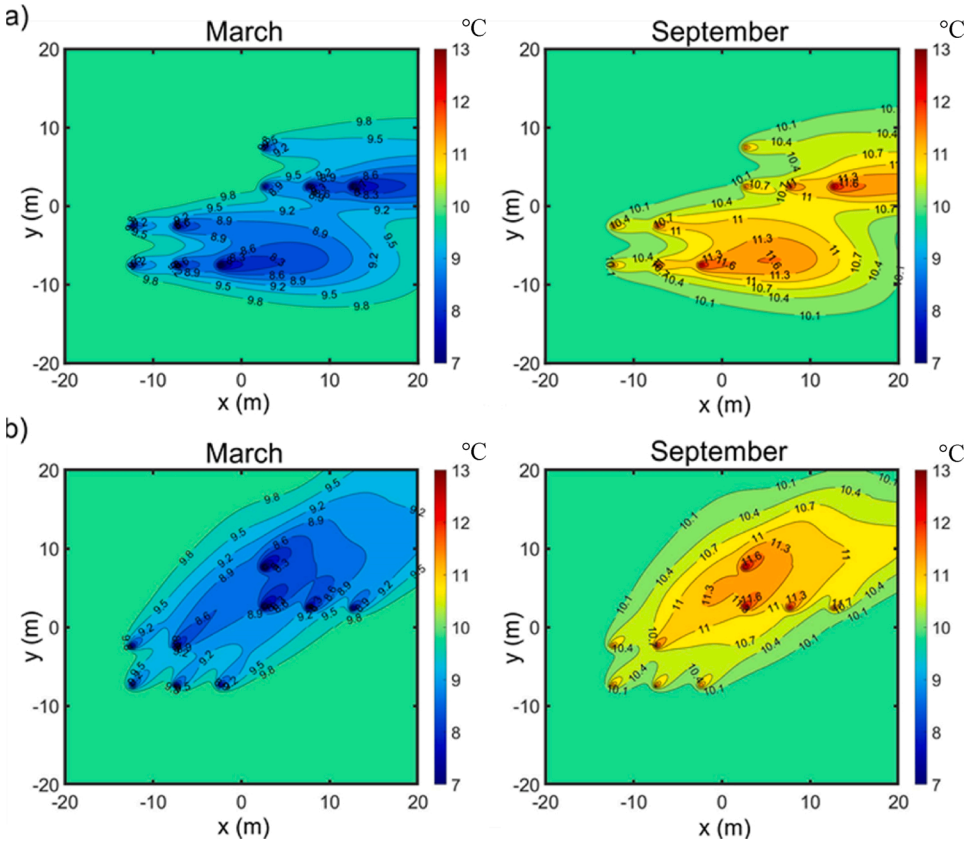

Fig. 10. Highlights on the thermal interactions for March and September. a) Case 1: groundwater flow along the *x*-axis; b) Case 2: groundwater flow making an angle 45° with the *x*-axis.

The figure also indicates that the thermal interaction between the two installations is essentially negligible, with some insignificant interactions in March, April and September. However, within the installations themselves, the thermal interaction between the heat sources can be considered significant. As it can be seen from this figure, the soil temperature in the area around the downstream heat sources for both installations has been affected by their upstream heat sources. In winter, the soil temperature in the downstream is lower than that in the upstream, and in summer it is higher. Fig. 10a highlights this for March, which marks the end of winter months; and September, which marks the end of summer months. Accordingly, the heat sources in the downstream would exhibit less energy efficiency compared to their upstream counterparts. Apparently, this sort of analyses is vital for engineers, who can during the design process avoid this kind of thermal interactions simply by deploying different configurations and distancing.

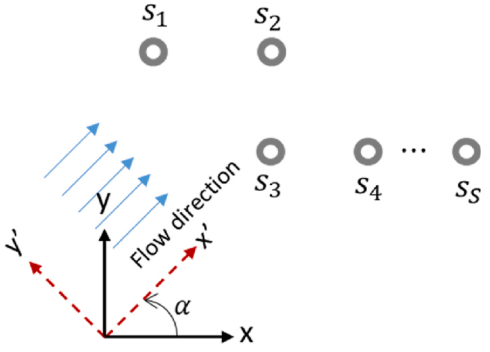

Fig. 11. Rotation of axis for groundwater flow making an angle α with the x-axis.

Case 2:groundwater flow making an angle 45° with the *x*-axis

In this case the groundwater is assumed to flow at an angle 45° from the *x*-axis. As indicated in Section 2, the governing heat equation, Eq. (1), is explicitly formulated based on a fluid flow along the x-axis, and hence this case cannot directly be analyzed by the solution given in Eq. (7). To tackle this issue, we apply the rotation of axes technique to map the 2D *xy* -Caterisan coordinate system to an *x'y'* -Cartersain coordinate system making an angle equal to the angle of the fluid flow, α, as shown in Fig. 11. In a matrix form, the rotation of axes is expressed as

$$\begin{bmatrix} x' \\ y' \end{bmatrix} = \begin{bmatrix} \cos\alpha & \sin\alpha \\ -\sin\alpha & \cos\alpha \end{bmatrix} \begin{bmatrix} x \\ y \end{bmatrix} \tag{27}$$

Fig. 12 shows the computed temperature distribution for Case 2, for 12 months. As for Case 1, the temperature distribution and the size of the affected area of the soil mass fluctuate significantly with the operating scenario of the months. Also, the motion of cold and hot plumes in times when the operation stops or changes modes is apparent. The difference with Case 1, however, is in the thermal interaction between the two installations. As the fluid is moving from GSHP 1 directly towards GSHP 2, the soil mass around GSHP 2 gets cooler in winter and hotter in summer. This can be seen in March and April, and in August and September, respectively. However, within the individual installations, the thermal interaction is less significant. Fig. 10b highlights this for March and September. It can be seen that the areas at the vicinity of the downstream heat sources are not much affected by their upstream counterparts. Remarkably, comparing Fig. 10a for Case 1 to Fig. 10b for Case 2 it can be noticed that downstream heat sources which have been affected by thermal interactions in Case 1 are almost not affected in Case 2. Evidently, this kind of analysis can be of significant importance to geothermal engineers, who can employ different grid configurations to make the best use of the direction of the groundwater flow.

Case 3:GSHP 1 extracting ± 75 W/m instead of ± 50 W/m

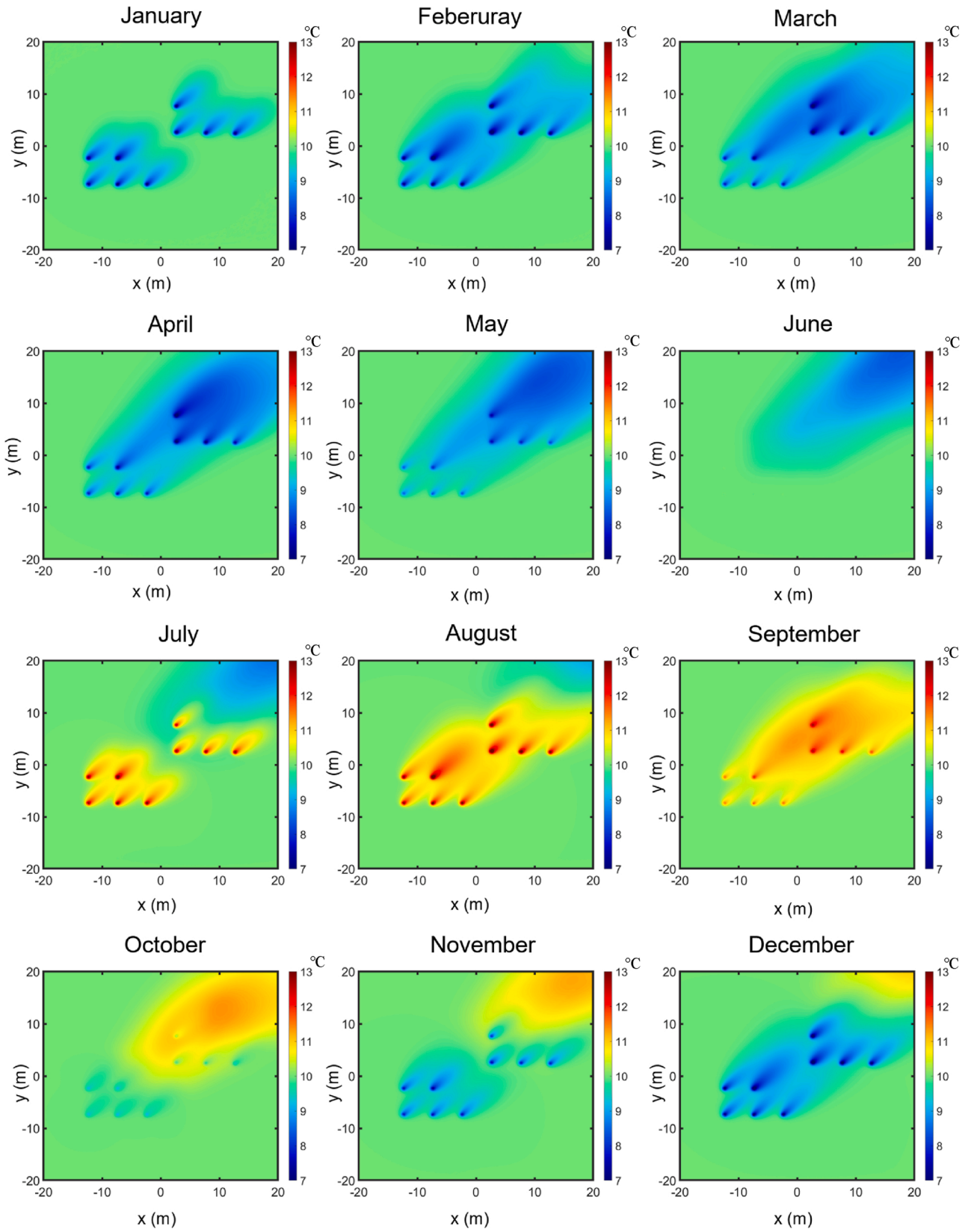

Fig. 12. Monthly temperature distribution for Case 2: groundwater flow making an angle 45° with the *x*-axis.

This case is introduced to highlight one of the engineering problems in regional ground source heat pump systems where one or more installations with larger power are constructed at the upstream of existing installations. This kind of problems can lead to unfair mining of geothermal energy, rapid depletion of the energy source, declining energy efficiency of the downstream installations and triggering conflicts among users.

Here we assume the same setup as for Case 2 except that the thermal

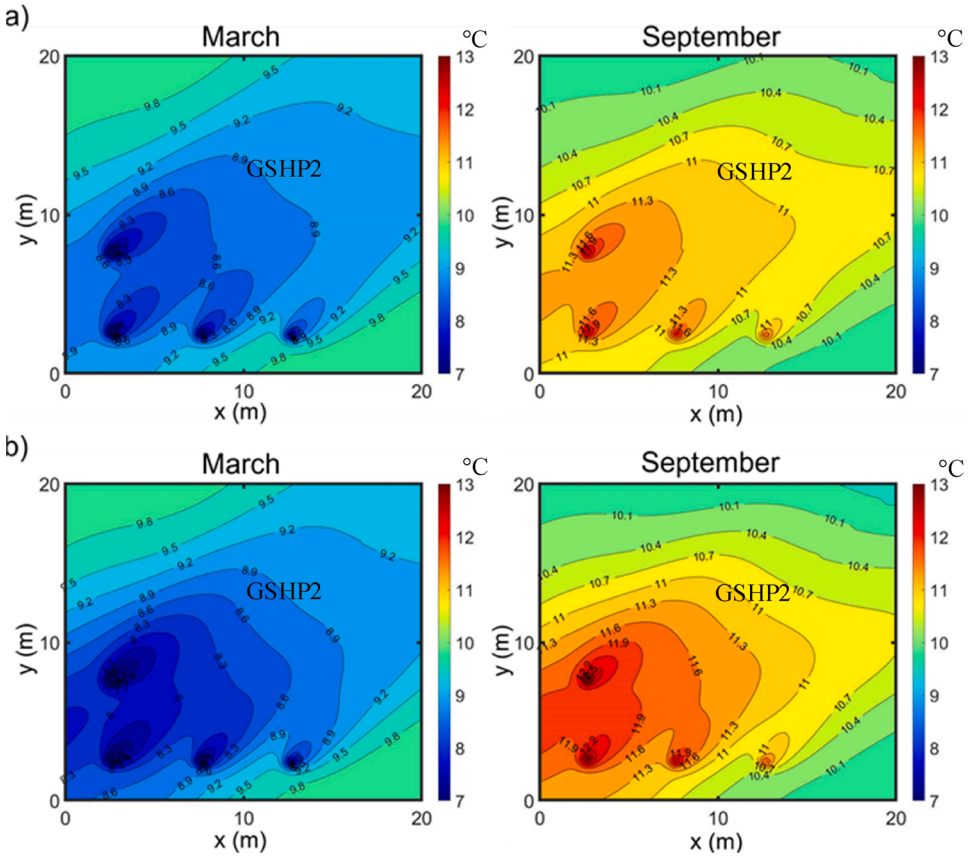

Fig. 13. Temperature distribution around GSHP 2. a) GSHP 1 operating with ± 50 W/m; b) GSHP 1 operating with ± 75 W/m.

loads of the heat sources in GSHP 1 are designed to use ± 75 W/m (instead of ± 50 W/m) and those for GSHP 2 remain using ± 50 W/m. Fig. 13 shows the temperature contours in March and September around GSHP 2 for two cases: a case in which GSHP 1 is operated with ± 50 W/m (as in Case 2), and a case in which GSHP 1 is operated with ± 75 W/m. Apparently, in the latter case the soil mass at the vicinity of GSHP 2 exhibits lower temperature in March and higher temperature in September, that would eventually reduce its energy efficiency.

6. Conclusions

Heat convection due to groundwater flow can have a significant effect on the amount of energy gained from the ground source heat pump (GSHP) system; a booming technology for yielding thermal energy from shallow depths of the earth to be utilized for heating and cooling of buildings. Despite its advantage as a non-intermittent technology, its excess use in highly populated areas can bring in undesirable thermal interferences between neighboring installations, leading eventually to rapid depletion of the energy sources, unfair mining of geothermal energy, declining long-term energy efficiency of the heat pumps and causing conflicts among users. This becomes more challenging in the presence of groundwater flow. As a result, the grid configuration and distances between neighboring GSHP systems have recently become important design criteria. This paper addresses this issue and introduces an analytical model for conductive-convective heat flow in an infinite domain subjected to multiple cylindrical heat sources. The spectral analysis is utilized to solve the governing heat equation for a single heat source; and the superposition principle is utilized to couple the combined effect of neighboring heat sources and installations. The proposed spectral model is formulated such that it is applicable to any random input thermal load signals and any arbitrarily configured heat source grids; all made in a highly efficient CPU time and capacity.

The verification and numerical examples demonstrate the computational capabilities of the model and highlight important physical characteristics of the GSHP system in the presence of groundwater flow. One of the main issues that concerns geothermal engineers is the thermal interaction between neighboring borehole heat exchangers and installations that can significantly affect the energy efficiency of the involved systems. The proposed model provides the computational means to easily modify the grid configurations based on the ground water flow direction in order to make optimal use of the subsurface energy sources. It enables analyzing the effect of excessive mining of geothermal energy in populated neighborhoods, and facilitates mitigating the rapid depletion of geothermal energy sources. The model has a relatively simple formulation and can easily be incorporated in engineering computational tools.

Declaration of Competing Interest

The authors declare that they have no known competing financial interests or personal relationships that could have appeared to influence the work reported in this paper.

References

Al-Khoury, R., 2012. Computational Modeling of Shallow Geothermal Systems. CRC Press/Balkema, The Netherlands.

Al-Khoury, R., BniLam, N., Arzanfudi, M.M., Saeid, S., 2020. A spectral model for a moving cylindrical heat source in a conductive-convective domain. Int. J. Heat Mass Transf. 163, 120517.

Al-Khoury, R., Bonnier, P.G., Brinkgreve, R., 2005. Efficient finite element formulation for geothermal heating systems. Part I: steady state. Int. J. Numer. Methods Eng. 63, 988–1013.

Arzanfudi, M.M., Al-Khoury, R., Sluys, L.J., Schreppers, G.M.A., 2020. A thermo-hydro-mechanical model for energy piles under cyclic thermal loading. Comput. Geotech. 125, 103560.

BniLam, N., Al-Khoury, R., 2016. Transient heat conduction in an infinite medium subjected to multiple cylindrical heat sources: an application to shallow geothermal systems. Renew. Energy 97, 145–154.
Capozza, A., De Carli, M., Zarrella, A., 2013. Investigations on the influence of aquifers on the ground temperature in ground-source heat pump operations. Appl. Energy 107, 350–363.
Carslaw, H.S., Jaeger, J.C., 1959. Conduction of Heat in Solids, second ed. Oxford University Press.
Cimmino, M., Baliga, B.R., 2019. A hybrid numerical-semi-analytical method for computer simulations of groundwater flow and heat transfer in geothermal borehole fields. Int. J. Thermal Sci. 142, 366–378.
COMSOL Multiphysics® v.5.4. www.comsol.com. COMSOL AB, Stockholm, Sweden.
Diao, N., Li, Q., Fang, Z., 2004. Heat transfer in ground heat exchangers with groundwater advection. Int. J. Therm. Sci. 43, 1203–1211.
Doyle, J.F., 1997. Wave Propagation in Structures: Spectral Analysis Using Fast Discrete Fourier Transforms. Springer-Verlag, New York, Inc.
Erol, S., Hashemi, M.A., François, B., 2015. Analytical solution of discontinuous heat extraction for sustainability and recovery aspects of borehole heat exchangers. Int. J. Therm. Sci. 88, 47–58.
FEFLOW: https://www.mikepoweredbydhi.com/products/feflow (Accessed October 2020).
Nabi, M., Al-Khoury, R., 2012a. An efficient finite volume model for shallow geothermal systems. Part I: model formulation. Comput. Geosci. 49, 290–296.
Nabi, M., Al-Khoury, R., 2012b. An efficient finite volume model for shallow geothermal systems—Part II: verification, validation and grid convergence. Comput. Geosci. 49, 297–307.
Nam, Y., Ooka, R., Hwang, S., 2008. Development of a numerical model to predict heat exchange rates for a ground-source heat pump system. Energy Build. 40, 2133–2140.
Pasquier, P., Marcotte, D., 2013. Efficient computation of heat flux signals to ensure the reproduction of prescribed temperatures at several interacting heat sources. Appl. Therm. Eng. 59, 515–526.
Pruess, K., Oldenburg, C., Moridis, G., 1999. TOUGH2 User's Guide, Version 2.0. Lawrence Berkeley National Laboratory Report LBNL-43134. Berkeley, CA, November 1999.
Yavuzturk, C., Spitler, J.D., Rees, S.J., 1999. A transient two-dimensional finite volume model for the simulation of vertical U-tube ground heat exchangers. ASHRAE Trans. 105 (2), 527–540.